GNSS-based tomographic reconstruction of the ionospheric electron density distribution using a combined algorithm

Wen Debao[1,2,*], Kefei Zhang[2] and Robert Norman[2]

[1]School of Traffic and Transportation Engineering,
Changsha University of Science & Technology,
Changsha 410004, China
[2]Center for Satellite Positioning and Navigation,
RMIT University, Melbourne 3001, Australia

An algorithm is proposed to image ionospheric electron density (IED) distribution. In this method, generalized singular value decomposition (GSVD) is first used to resolve the ill-conditioned problem in the computerized ionospheric tomography system. Its estimate is then provided as the initial approximation required by the improved algebraic reconstruction technique (IART). Numerical simulation has demonstrated that the combined algorithm is superior to both GSVD and IART for tomographic inversion of IED. Finally, the method is applied to perform inversion of IED using a set of global navigation satellite system (GNSS) data during a magnetically disturbed period. The reconstructed results reveal two prominent features of the ionosphere under the disturbed condition. The reliability of the method is also validated by the ionosonde data recorded at Wuhan station, China.

Keywords: Combined algorithm, computerized ionospheric tomography, imaging reconstruction, ionosphere, total electron content.

VARIABILITY in solar radiation levels and geomagnetic activity causes fluctuations in the ionosphere that affect satellite navigation and positioning, communications and satellite altimetry. An improved understanding of the physics of the ionosphere requires a global, dynamical view of the ionosphere[1]. Computerized ionospheric tomography (CIT) technique, which is a subset of remote sensing, has been proposed and has gained popularity in the ionospheric imaging community over the past two decades as an efficient means of obtaining a global view of this variability[2]. From then on, various theoretical studies[3–6] and experiments[7] have been carried out by means of the measurement data of polar orbit satellites, such as the navy navigation satellite system. Since the ground receivers are often installed along a fixed longitude chain, the above studies can only image the two-dimensional ionospheric structure in the altitude–latitude cross-section. In recent years, the global navigation satellite system (GNSS)-based CIT technique has received more attention, since it may be used to reconstruct the ionospheric structure in three-dimensional mode[8–17]. However, from a tomographic perspective, the restricted view of the imaging system, coupled with the irregularity and sparsity of ground GNSS stations, makes it inherently prone to data insufficiency and the inversion process one of the most challenging cases of limited data tomography. Therefore, tomographic reconstruction of the ionospheric electron density (IED) distribution is an ill-conditioned inverse problem.

To resolve the above problem, numerous algorithms have been presented in recent years. On the whole, they can be divided into two categories: the iterative reconstruction algorithm and the other is the non-iterative reconstruction algorithm. The improved algebraic reconstruction technique (IART)[18] is one of the iterative methods which is simple and highly efficient in computation. It resolves the ill-conditioned problem by incorporating some prior information into each voxel used in an ionospheric tomography system. For those voxels without any ray path traversing through them, IART compensates for the incomplete data using a good initial approximation for the overall distribution. This means that IART is sensitive to the initial approximation. In the non-iterative reconstruction algorithms, the generalized singular value decomposition (GSVD) method is popular for solving the ill-conditioned inverse problem in ionospheric tomography. One of advantages of GSVD is that the reconstruction quality does not depend on the initial approximation, because its solution can be calculated directly from total electron content (TEC) data without any initial estimates. But its solution is usually an approximate due to the limitations in the available information and the impacts of discretized errors and observation noises[15].

In view of the disadvantages of the above tomographic algorithm, a tomographic algorithm is presented here to improve the accuracy of inverse results. The method is a combination of the GSVD method and the IART algorithm. In this combined algorithm, GSVD is first applied to solve the ill-conditioned inverse problem of the ionospheric tomography system. Taking into account the 'coarse' of the solution, the estimates of GSVD are then input as the initial approximation of the IART to be further improved in an iterative manner. The feasibility of the combined algorithm is confirmed by a numerical simulation experiment. It is then successfully used to reconstruct the IED imaging from the actual GNSS data in China, and the reliability of the reconstructed results is also validated by ionosonde data recorded at Wuhan station, China[15].

As discussed in Austen *et al.*[2], one measurable parameter of the ionosphere is TEC, which is the line integral of the electron density along the ray path. It can be mathematically represented as

$$\mathrm{TEC} = \int_p N(s)\,\mathrm{d}s, \tag{1}$$

*For correspondence. (e-mail: wdbwhigg@163.com)

where $N(s)$ represents IED, and p the ray propagation path between a satellite and a receiver. The CIT technique applies TEC to invert electron density distribution of the ionosphere. To simplify the IED inversion, the imaged region of the ionosphere is first divided into small voxels in a selected reference frame. Within each voxel, the electron density can be assumed to be constant. So the TEC along the ray path can be represented as a finite sum of shortest integrals along different segments of the ray path. The reconstruction problem then centres on solving the following system of equations:

$$\mathrm{TEC}_i = \sum_{j=1}^{n} A_{ij} x_j + e_i. \tag{2}$$

Equation (2) can be generally written in a simple matrix notation as:

$$y_{m\times l} = A_{m\times n} x_{n\times l} + e_{m\times l}, \tag{3}$$

where n is the number of voxels in the image, m the number of TEC measurements, y a column vector of m known TEC measurements, A a matrix containing all the lengths of the m ray paths traversing the corresponding n voxels, x the vector consisting of all the unknown electron densities in all the voxels, and e is a column vector associated with the discretization errors and measurement noises.

Tomographic reconstruction of IED is an inverse problem in which the unknown x is estimated from the known A and y. As described earlier, some limitations in ionospheric tomography often make this reconstruction an ill-conditioned inverse problem. In such a case, small perturbations of y in eq. (3) make the solution large perturbations. Such a problem may be handled with GSVD. GSVD is a generalization of the singular value decomposition technique, which can be used to solve the damp least square problem as proposed by Tikhonov. This approach looks for the solution of the following problem[19]:

$$\min_{x\in\varphi} \| Ax - y \|^2 + \alpha \| Lx \|^2, \tag{4}$$

where α is the regularization parameter and L a positive definite matrix which takes different forms according to the order of regularization. For zero-order Tikhonov regularization, L is the identity matrix and for first-order Tikhonov regularization:

$$L = \begin{pmatrix} -1 & 1 & 0 & . & . & 0 \\ 0 & -1 & 1 & 0 & . & 0 \\ . & . & . & . & . & . \\ . & . & . & . & . & . \\ 0 & . & . & . & -1 & 1 \end{pmatrix}, \tag{5}$$

where L is a $p \times n$ matrix, and the rank of L is p.

Using the GSVD method, the matrices $A_{m\times n}$ $(m \geq n)$ and $L_{p\times n}$ $(n \geq p)$ can be written as[19]:

$$A = U \begin{pmatrix} \Lambda & 0 \\ 0 & I_{n-p} \end{pmatrix} B^{-1}, \tag{6}$$

and

$$L = V(C \;\; 0)B^{-1}, \tag{7}$$

where U is an $m \times n$ orthogonal matrix, B an $n \times n$ non-singular matrix. Λ a $p \times p$ diagonal matrix and C is also a $p \times p$ diagonal matrix.

The Tikhonov regularized solution can then be written as:

$$x_{\alpha,L} = (A^T A + \alpha L^T L)^{-1} A^T y, \tag{8}$$

In the damped least square approach, the value of α is unspecified. The indeterminacy of α can be eliminated by the method of generalized cross-validation which can be represented as:

$$G(\alpha) = \frac{\| Ax_{\alpha,L} - y \|^2}{\mathrm{trace}(I - A(\alpha))^2}. \tag{9}$$

Additional constraint can solve the ill-conditioned problem in ionospheric tomography system. However, for each voxel the electron density value obtained from GSVD is only an approximation due to the existence of discretization errors and GNSS measurement noises and the limitation of available TEC data. Taking into account the approximate characteristics of the solution of GSVD, IART is used to improve the accuracy of the solution. The procedure is described below.

The estimates obtained from eq. (8) are input as the initial states of IART[18].

$$x^{(0)} = x_{\alpha,L}. \tag{10}$$

Next the reconstruction is performed with the IART algorithm:

$$x^{(k+1)} = x^{(k)} + \lambda_k (y_i - a_i x^{(k)}). \tag{11}$$

The column vector λ_k composed of all relaxation parameters is given as:

$$\lambda_k = g^k (a_i \cdot g^k), \tag{12}$$

where $g^k = [g_1^k, g_2^k, ..., g_n^k]^T$, and $g_i^k = a_{ij} x_j^k$, a_i represents the ith row vector in projection matrix A, and γ is fixed in ionospheric tomography.

Let us consider numerical experiments using simulated data. Before the combined algorithm is applied to reconstruct the electron density distribution using actual TEC data, it is necessary to confirm its feasibility and reliability using simulated TEC data. The simulated data are generated from the IRI 2001 model. In this model, IED is varies smoothly and is available from 50 to 2000 km. The simulation procedure is summarized as follows.

(i) In a selected reference frame and time period, the actual positions of GNSS satellites and ground receivers are used to create the projection matrix A. In this simulation, 48 GNSS receivers over China are used.

(ii) The ionospheric electron density at the centre of each voxel is generated from the IRI 2001 model and considered as the initial electron density value of the corresponding voxel. The simulated time period is 01 : 30–02 : 00 UT on 8 July 2002 along east longitude 106°. The discretized density distribution is represented by x_{simu}, and then the simulated TEC measurement y_{simu} without noise is computed using the following equation:

$$y_{\text{simu}} = A \cdot x_{\text{simu}}. \tag{13}$$

(iii) Practically, a small amount of random noise e_{simu} should be added to the simulated TEC values y_{simu}. One can then obtain:

$$y_{\text{nois}} = y_{\text{simu}} + e_{\text{simu}}. \tag{14}$$

(iv) Using the above procedure, the GSVD is used to invert IED from TEC measurements with noise. Its estimate x_{est} is then obtained.

(v) The estimates of GSVD are input as an initial state of IART, and it is then improved using eqs (11) and (12).

Figure 1 *a* illustrates IED distribution at 02 : 00 UT on 8 July 2002 along 106°E, which is obtained from the IRI 2001 model. The reconstructed electron density distribution using the combined algorithm is plotted in Figure 1 *b*. Comparing Figure 1 *b* with *a*, it can be seen that the ionospheric structure is reconstructed well as a whole. The average density error is 8.7×10^9 el/m^3, which is very small compared with the typical peak density of 1.09×10^{12} el/m^3. The statistical results show that the IED image is reconstructed with sufficiently high accuracy using the simulated TEC data. This demonstrates the feasibility of reconstructing IED using the combined algorithm.

In order to demonstrate the advantages of the combined reconstruction algorithm to GSVD alone or IART alone,

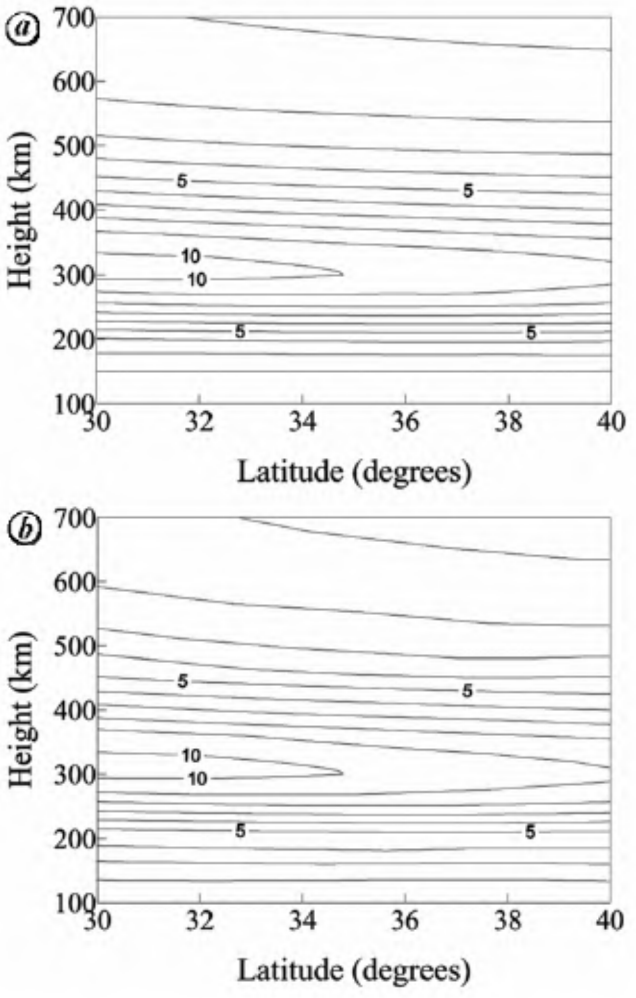

Figure 1. Contour plots of the modelled and reconstructed electron density distributions at east longitude 106°. ***a***, Modelled electron density distribution with the IRI 2001 model. ***b***, Reconstructed electron density distribution with the combined reconstruction algorithm (the unit of ionospheric electron density (IED) is 10^{11} e/m^2).

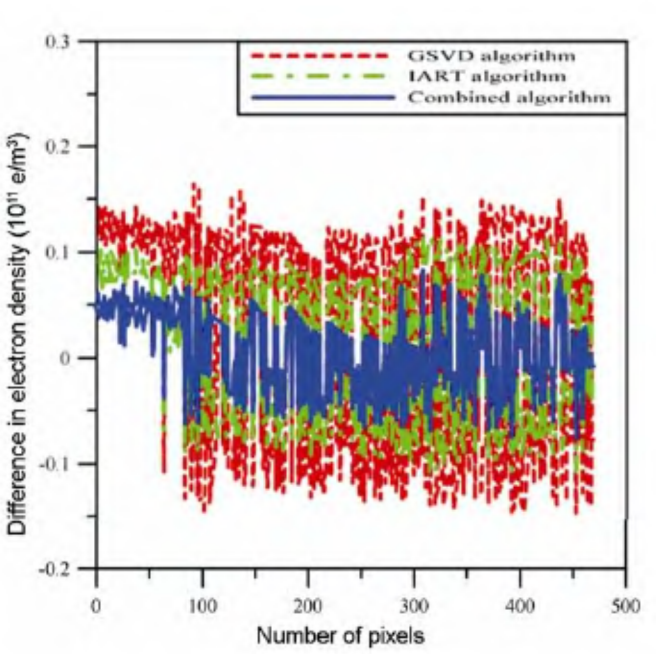

Figure 2. Comparison of the difference between the reconstructed electron density distributions of the three algorithms and those obtained from the IRI 2001 model.

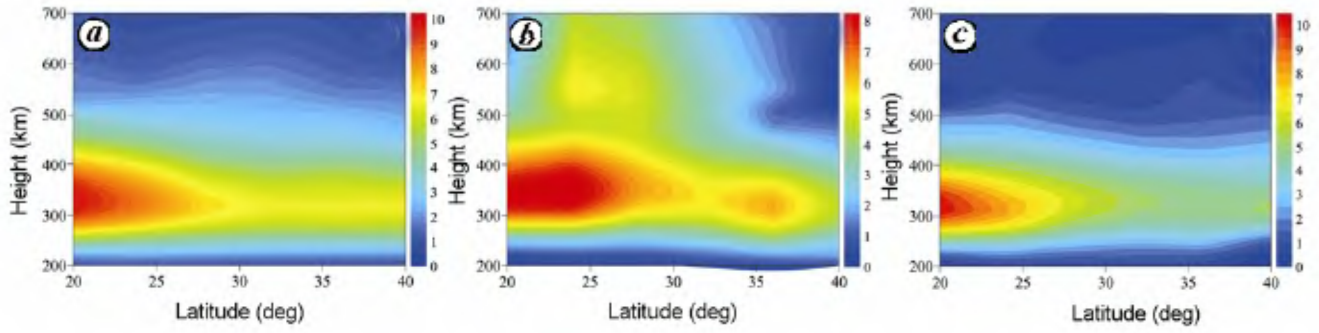

Figure 3. Two-dimensional images of IED over China at 23 : 00 BT on magnetic quiet days (***a***, 20 August 2003 and ***c***, 22 August 2003) and storm day (***b***, 21 August 2003). (The unit of IED is 10^{11} e/m^3.)

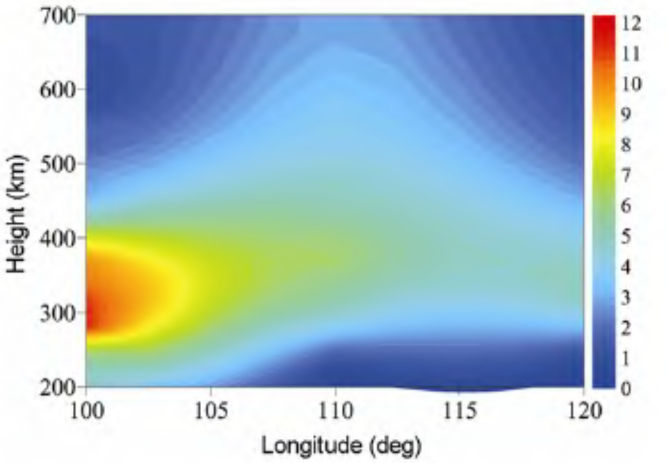

Figure 4. Contour plots of IED over the longitude and altitude cross-section at 30.5°N and at 15 : 00 UT on 21 August 2003. (The unit of IED is in 10^{11} e/m^3.)

Figure 2 compares the difference between the reconstructed IED distributions using each algorithm mentioned above and those obtained from the IRI 2001 model. From Figure 2, one can see that the difference between IEDs inverted from the combined algorithm and those obtained from the IRI 2001 model is minimum in the above three algorithms. This indicates that the combined algorithm is superior to both GSVD and IART in performing ionospheric tomography and it can be applied to improve the quality of the imaging reconstruction.

Now let us consider experiments using actual observation data. With TEC data derived from actual GNSS data, the combined algorithm is applied to reconstruct the corresponding electron density distributions. GNSS pseudoranges of low elevation angle satellites are sensitive to multipath effects: in general, the lower the elevation angle, the larger the multipath error. On the other hand, GNSS data obtained at low elevation angles are important for getting some information about the vertical distributions of IED. Hence, a crucial problem is how to select a proper elevation mask angle for the CIT technique. A large elevation mask angle reduces the vertical resolution of the inverted results; a small elevation angle reversely affects the accuracy of IED inversion[20]. In this study, an elevation mask angle of 10° is adopted. The reconstruction algorithm includes the capability to automatically reject GNSS data of elevation angle less than 10° even if ray paths may intersect the image plane. In this study, GNSS observation data, which are recorded from 14 : 30 UT to 15 : 00 UT (22 : 30 BT–23 : 00 BT, BT represents Beijing time) on 21 August 2003 and obtained from the Crustal Movement Observation Network of China, are used to study the variation of IED under magnetically disturbed condition. This specific period is selected here because it can show some typical structures of the ionosphere.

Figure 3 shows the variations of IED with altitude and latitude along east longitude 114.5° at 15 : 00 UT (23 : 00 BT) during the magnetically active period on 21 August 2003 and magnetically quiet periods on 20 and 22 August 2003. Comparing Figure 3 *b* with *a*, one can see that IED in the F region is depleted during the geomagnetic storm on 21 August 2003, which appears as negative storm-phase effects. The maximum depletion of the IED reaches 30%. The positive storm phase effects of the ionosphere however appear latitudinally from 20°N to 37°N and altitudinally from 500 to 700 km above the ground, and then the negative storm phase effects also appear latitudinally from 37°N to 40°N. The reconstructed results show that the storm-phase effects are not only latitude-dependent but also altitude-dependent. Similar characteristics of the geomagnetic storm can also be found in other time periods. In Figure 3 *b*, a clear ionospheric trough at 32°N can also be seen. IED value of the trough is about 5.7×10^{11} e/m^3. Further moving towards the north, IED increases and reaches a peak at 36°N, where the peak height is about 320 km and the peak density of the ionosphere increases to 6.2×10^{11} e/m^3, and then IED begins to decrease. However, the peak IED reaches 8.0×10^{11} e/m^3 south of the trough, and the peak height is about 350 km, which is higher than the peak height at the north of the ionospheric trough. Meanwhile, an intensively disturbed structure of the ionosphere

appears between 20°N and 35°N. From Figure 3 *c*, it can be seen that IED gradient gradually comes back to the state before the storm occurred.

Figure 4 illustrates IED variation with the longitude and height at 30.5°Nand 23 : 00 BT. A clearly disturbed structure of the ionosphere can also be seen in this cross-section. Figures 3 *b* and 4 demonstrate that the combined algorithm may be effectively used to reconstruct and study large-scale ionospheric structure under disturbed conditions.

To validate the reliability of the tomographic results, both the NmF2 and hmF2 values obtained from ionosonde observations at Wuhan Station are compared with those inverted by GNSS-based tomographic reconstruction. The peak height hmF2 and the peak density NmF2 obtained from the ionosonde observations and GNSS-based tomographic results on 21 August 2003 are shown in Figures 5 and 6 respectively. Comparison shows that there is good agreement between the results from the ionosonde data and the tomographic data as a whole. This confirms that a reliable IED distribution during the magnetic storm on 21 August 2003 can be reconstructed using the GNSS-based CIT technique.

The available ionosonde data at Wuhan station provide an independent comparison of the electron density profile reconstructed from actual GNSS observations. Figure 7 illustrates the comparison of the reconstructed electron density profile with that obtained from ionosonde data recorded at Wuhan station at 15 : 00 UT on 21 August 2003. It shows that the tomographically reconstructed profile agrees with that obtained from ionosonde data. From Figure 7, it can be seen that the inverted electron density values are larger than those obtained from the ionosonde data above 200 km altitude. However, the inverted electron density values are smaller than those obtained from ionosonde data between 100 and 200 km in altitude. The agreement of the two ionospheric electron density profiles further validates the reliability of the GNSS-based tomographic results.

The combined method is presented here and applied to the reconstruction of IED from TEC measurements,

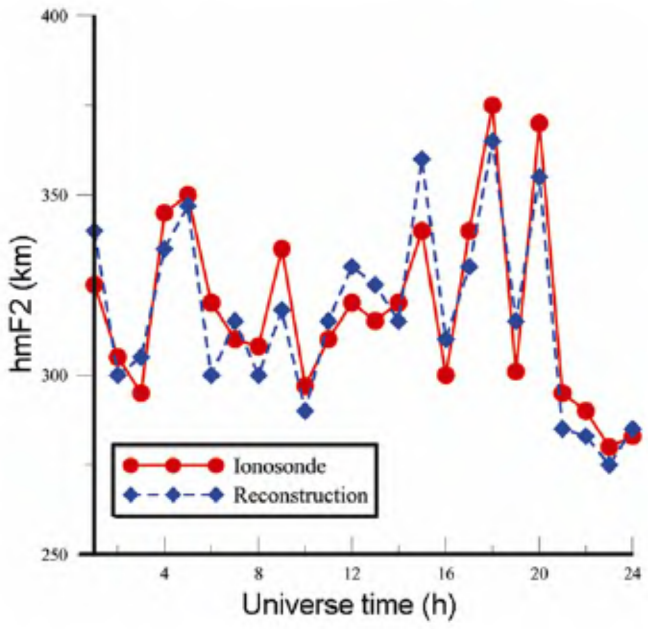

Figure 5. Comparison of hmF2 values obtained from GNSS-based CIT technique and those from ionosonde data recorded at Wuhan station.

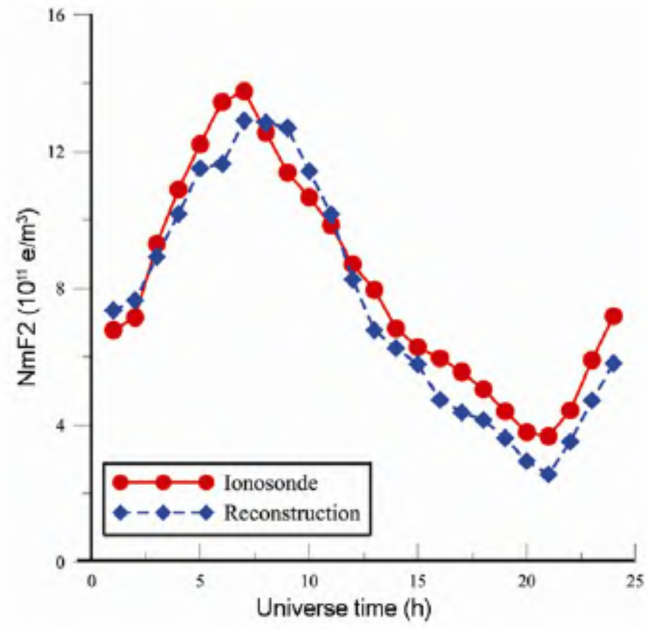

Figure 6. A comparison of NmF2 values obtained from GNSS-based CIT technique and those from ionosonde data.

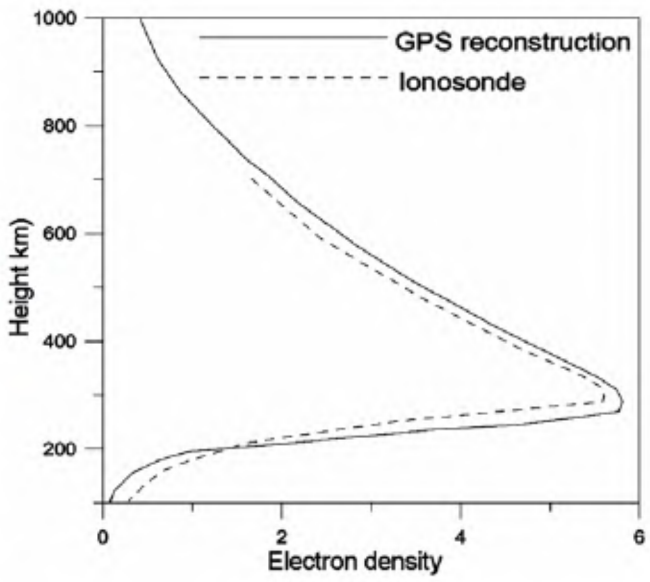

Figure 7. Comparison of IED profile reconstructed from GPS data with that obtained from ionosonde data recorded at Wuhan station. (The unit of IED is 10^{11} e/m^3).

which is derived from GNSS data. The feasibility of this method has been demonstrated using computer simulation, in which the ideal density distributions are provided with TEC generated from the IRI 2001 model. The simulated results show that the main ionospheric structures are reconstructed well. This means that a smaller noise cannot bring out a large effect on the tomographic reconstruction of IED using the combined algorithm. Meanwhile, simulated reconstruction results show that the combined method is superior to both GSVD and IART in performing ionospheric tomography. After the simulated results are validated, the combined method is then applied to reconstruct a large-scale structure of the ionosphere during a magnetically disturbed period, and the reconstructed results illustrate some significant features of the ionosphere, such as ionospheric troughs and ionospheric disturbed structure. The tomographic results are also validated using ionosonde data observed at Wuhan station.

Although the computation of the combined algorithm is a little longer than that of GSVD or IART alone, when it is applied to reconstruct IED images, it is negligible for a high-performance computer with respect to the quality of the reconstructed ionospheric image. In addition, the main aim of this work is to get the three-dimensional image of the ionosphere by means of GNSS-based CIT technique. The temporal evolution of IED is not considered here. In future work, this method would be extended to a fully four-dimensional tomographic reconstruction by considering the temporal evolution of the ionosphere.

1. Howe, B. M., Runciman, K. and Secan, J. A., Tomography of the ionosphere: 4-dimensional simulations. *Radio Sci.*, 1998, **33**, 109–128.
2. Austen, J. R., Franke, S. J. and Liu, C. H., Ionospheric imaging using computerized tomography. *Radio Sci.*, 1988, **23**, 299–307.
3. Raymund, T. D., Austen, J. R., Franke, S. J., Liu, C. H., Klobuchar, J. A. and Stalker, J., Application of computerized tomography to the investigation of ionospheric structure. *Radio Sci.*, 1990, **25**, 771–789.
4. Na, H. and Lee, H., Resolution analysis of tomographic reconstruction of electron density profiles in the ionosphere. *Int. J. Imag. Syst. Technol.*, 1990, **2**, 209–218.
5. Fremouw, E. J., Secan, J. A. and Howe, B. M., Application of stochastic inverse theory to ionospheric tomography. *Radio Sci.*, 1992, **27**, 721–732.
6. Kunitsyn, E. V. and Tereshchenko, E. D., Radio tomography of the ionosphere. *IEEE Trans. Antennas Propag. Magnetism*, 1992, **34**, 22–30.
7. Pryse, S. E. and Kersley, L., A preliminary experimental test of ionospheric tomography. *J. Atmos. Sol.-Terr. Phys.*, 1992, **54**, 1007–1023.
8. Leitinger, R., Ladreiter, H. P. and Kirchengast, G., Ionospheric tomography with data from satellite reception of global navigation satellite system signals and ground reception of navy navigation satellite system signals. *Radio Sci.*, 1997, **11**, 1657–1669.
9. Rius, A., Ruffini, G. and Cucurull, L., Improving the vertical resolution of ionospheric tomography with GNSS occultation. *Geophys. Res. Lett.*, 1998, **24**, 2291–2294.
10. Bust, G. S., Coco, D. and Makela, J. J., Combined ionospheric campaign 1: ionospheric tomography and GNSS total electron content (TEC) depletions. *Geophys. Res. Lett.*, 2000, **27**, 2849–2852.
11. Mitchell, C. N. and Spencer, P. S., A three-dimensional time-dependent algorithm for ionospheric imaging using GNSS. *Ann. Geophys.*, 2003, **46**, 687–696.
12. Ma, X. F. and Maruyama, T., Three-dimensional ionospheric tomography using observation data of GNSS ground receiver and ionosonde by neural network. *J. Geophys. Res.*, 2005, **110**,
13. Fridman, S. V., Nickisch, L. J., Aiello, M. and Hausman, M., Real-time reconstruction of the three-dimensional ionosphere using data from a network of GNSS receivers. *Radio Sci.*, 2006, **41**, RS5S12.
14. Wen, D. B., Yuan, Y. B. and Ou, J. K., Monitoring the three-dimensional ionospheric electron density distributions using GPS observations over China. *J. Earth Syst. Sci.*, 2007, **11**, 6235–6244.
15. Wen, D. B., Yuan, Y. B., Ou, J. K. and Zhang, K. F., A hybrid reconstruction algorithm for three dimensional ionospheric tomography. *IEEE Trans. Geosci. Remote Sensing*, 2008, **46**, 1733–1738.
16. Wen, D. B., The research progress of computerized ionospheric tomography technique. *Bull. Natl. Sci. Found. China*, 2010, **24**, 17–20.
17. Wen, D. B. and Liu, S. Z., A new ionospheric tomographic algorithm – constrained multiplicative algebraic reconstruction technique (CMART), 2010, **119**, 489–496.
18. Wen, D. B., Yuan, Y. B., Ou, J. K., Huo, X. L. and Zhang, K. F., Three-dimensional ionospheric tomography by an improved algebraic reconstruction technique. *GNSS Solut.*, 2007, **11**, 251–258.
19. Bhuyan, K., Singh, S. B. and Bhuyan, P. K., Tomographic reconstruction of the ionosphere using generalized singular value decomposition. *Curr. Sci.*, 2002, **83**, 1117–1120.
20. Wen, D. B., Yuan, Y. B., Ou, J. K., Huo, X. L. and Zhang, K. F., Ionospheric temporal and spatial variations during the 18 August 2003 storm over China. *Earth Planet. Space*, 2007, **50**, 313–317.

ACKNOWLEDGEMENTS. This work is supported by the National Natural Science Foundation of China (Grant No. 40804002) and the Scientific Research Fund of Hunan Provincial Education Department (09B007), China. This research is partially supported by the Department of Innovation, Industry Science and Research through its Australian Space Research Program (ASRP) and the International Science Linkages (with both China and US) funding schemes awarded to K.Z. from RMIT University. We thank the Data Center for the Crustal Movement Observation Network of China for providing ground-based GNSS tracking station data. We also thank Prof. Libo Liu, Institute of Geology and Geophysics, Chinese Academy of Sciences, providing ionosonde data.

Received 25 August 2009; revised accepted 23 September 2010